Deorbiting Upper-Stages in LEO at EOM using Solar Sails

Alexandru IONEL*

*Corresponding author
INCAS – National Institute for Aerospace Research "Elie Carafoli",
B-dul Iuliu Maniu 220, Bucharest 061126, Romania,
alexandru.ionel@incas.ro

DOI: 10.13111/2066-8201.2017.9.2.9

Received: 04 April 2017/ Accepted: 21 May 2017/ Published: June 2017

Abstract: *This paper analyzes the possibility of deorbiting a launch vehicle upper-stage at end-of-mission from low Earth orbit through the use of a solar sail. Different solar sail sizes are taken into account. The analysis is made via a MATLAB numerical simulation, integrating with the ode45 solver the accelerations arising from geopotential, atmospheric drag and solar radiation pressure. Direct solar pressure and drag augmentation effect are analyzed and a state of the art study in the solar sail research field is performed for a better grasp of the feasibility of the device implementation.*

Key Words: *solar sail, launch vehicle upper-stage, MATLAB numerical simulation, solar radiation pressure, drag augmentation, orbital mechanics, orbital perturbation, ode45.*

1. LEO DEBRIS

Collisions and deliberate explosions, causing break-up events, represent the origin of the majority of space debris. The 1960s witnessed intentional destruction of spacecraft, by the use of antisatellite tests or self-destruct mechanisms. The intentional destruction of the Chinese Fengyun 1C satellite on January 11, 2007, constituent of a Chinese antisatellite test, and the unplanned collision of Iridium 33 and Cosmos 2251 on February 10, 2009, are considered of most importance in the expansion of the space debris population, and have added 3300 and 2200 fragments to the catalog of tracked objects, as well as hundreds of thousands of smaller fragments. Accidental explosions are mainly caused by residual onboard propellant, but also from collisions with other space debris. Because collisions are more destructive, they produce more debris objects than explosions. After debris is created following a break-up event, it follows different orbits, which modify with time. Objects in an orbit move with approximately the same speed, but not in the same direction. LEO orbital speed is mostly 7.5 km/s, but if a conjunction takes place (one object moving close to another), the relative velocity can reach 14 km/s. The majority of conjunctions happen at a 45 degree angle, with a 10 km/s relative velocity. Orbital debris sizes vary. The U.S. Space Surveillance Network (SSN) tracks and lists in a space object catalog the first category of debris sizes, namely objects approximately 10 cm in diameter. This tracking plays a major role in predicting conjunctions and satellite collision maneuvering. Depending on the shape of the debris objects, the SSN can track debris ranging from 5 to 10 cm in diameter, adding to a cataloged total of 22,000 objects. Objects down to 1 cm represent the next category in debris sizes, cannot be tracked, and have the potential of destroying a satellite or rocket body. 500,000 of these fragments are estimated in LEO, and a collision of a satellite or

rocket body with this debris size can result in tens of thousands of new debris objects. The third category of space debris is represented by 3 mm to 1 cm objects, also cannot be tracked, are in the number of millions in LEO, and in the case of a collision, can end a satellite's mission. The fourth category of space debris is marked by objects smaller than 3 mm, are estimated at a LEO population of about 10 million, can cause localized damage to spacecraft, and collision effects from them are dealt with through improved designs and shielding [1]. According to [2], in 2006 ASI, BNSC, CNES, DLR and ESA signed a "European Code of Conduct", which defined a set of suggested rules to prevent increasing the amount of space debris in the next years. This document led to the ESA's document "Requirements on Space Debris Mitigation for Agency Projects" on April 2008, which defines the rules to be followed by every future European mission. According to these rules, any European satellite within an altitude of 2000 km has to de-orbit in 25 years after the end of its mission (EOM). Hence, meeting this requirement is a driving parameter when designing a new mission in LEO. [3] evaluates techniques for end-of-life disposal of space assets: chemical propulsion maneuvers, low-thrust propulsion transfer, drag augmentation, and electrodynamic tethers. The success of the Japanese Space Agency (JAXA) in deploying and operating a solar sail on an interplanetary journey to Venus, clearly demonstrated that solar sailing is a feasible technology of interest for future scientific missions.

2. SOLAR SAILS AS DEORBITING DEVICES

Solar radiation pressure augmented deorbiting can provide a passive end-of-life solution, where a large reflective deployable structure is used to increase the spacecraft area-to-mass ration. Then, the combined effects of SRP and the geopotential perturbation cause an increase in orbital eccentricity to lower the orbit perigee and so induce air drag. [4] discusses the use of solar radiation pressure to passively remove small satellites from high altitude Sun-Synchronous orbits. An analytical model of the orbital evolution based on a Hamiltonian expressing the orbital evolution due to SRP and the J_2 effect, is developed, which is derived to calculate the minimum required area-to-mass-ratio to deorbit. One conclusion is that SRP-augmented deorbiting is most effective and reliable for Sun-synchronous orbits with semi-major axes between about 2000 km and 4500 km. Also, the numerical results are verified using Satellite Tool Kit (STK v9.2.2). The propagation in STK was performed with the HPOP propagator and including aerodynamic drag, the Earth gravitational harmonics up to 21st order, and third body perturbations by the Sun and the Moon in addition to SRP and the J_2 effect. Three different scenarios were tested, low altitude (1000 km), medium altitude (2300 km) and high altitude (4000 km). In the low altitude test, the spacecraft deorbited in 500 days, in the medium altitude test in 3.5 years and in the high altitude test in 1 year. Additionally, a foldable pyramid (FRODO) for CubeSat deorbiting is also discussed in the paper. In [2], the use of solar sails as devices to speed up the de-orbiting of LEO objects is considered. The 1999 DLR successful deployment test of a 20X20 meters square sail, NanoSail-D2, and the Gossamer solar sail activities roadmap are described. The first step of the Gossamer project is the deployment of a 5-by-5 meters solar sail in Earth orbit, to demonstrate the capabilities of manufacturing, packaging and successfully deploy in space a fully scalable system. The evolution with Gossamer-2 will be testing in Earth orbit preliminary attitude and orbit control using the solar radiation pressure as the only source for the required control torques. Finally, a full scale interplanetary mission is intended to be realized as the third step of the program, Gossamer-3. For the orbital dynamics formulations, Cowell's formulation was used, for the expression of the gravitational perturbation, the

effect of the non-symmetric mass distribution was taken into consideration using the well-established spherical harmonics representation, up to J_3 contribution. Also, solar radiation pressure perturbation, third body perturbation and atmospheric drag expressed with the Harris-Priester model were taken into account. The main test case scenario in the numerical simulation considered the following conditions: orbit: Dawn-Dusk Sun Synchronous Orbit at 620 km altitude; total satellite mass: 140 kg; sail area: 25 m^2; atmospheric density model: Harris-Priester. As conclusions, the spacecraft re-enters the atmosphere after 390 days, Figure 1. The deorbiting time may double when the solar flux parameter F10.7 is slightly modified. A proper attitude maneuver mechanization is proposed in [5] to harvest highest solar drag for Earth orbiting satellites. The maneuver is realized using a to-go quaternion calculated from body fixed frame measurements. The sail normal direction is calculated using quaternion rotations, and this with the current normal direction are used to find the to-go quaternion for attitude control. Nonlinear attitude control of the spacecraft is carried out using a positive definite Lyapunov function. For the numerical simulations, the equation of the orbital motion of the satellite is represented with respect to the Earth centered inertial coordinate system. Only a simple gravitational field without the spherical harmonics is considered. The mass of the satellite was considered to be 6 kg and the solar sail area 25 square meters. In all the simulation cases, the satellite is initially assumed to be in a circular orbit with 42000 km semi major axis. Three simulation cases are considered, an equatorial orbit, and 45 and 90 degrees inclination orbits. For the las two cases, the right ascension of ascending nodes are taken as 90 degrees. As conclusion, it is shown that, in each case, the maximum solar drag is successfully obtained with the method developed, resulting in similar orbital decays all three cases. [3] studies the dynamics of deorbiting a nano-satellite by using a solar sail, considering in the dynamic modeling multiple space environment perturbations and also obtaining approximated analytical solutions and numerical simulations of the perturbation torques. The dimension of the nano-satellite is 0.1 x 0.1 x 0.1 m^3, and the square solar sail is 5 x 5 square meters. In the numerical simulations, for the orbital dynamics, the Gaussian perturbation equation is used to describe the orbital motion in a geocentric inertial frame of Earth. The perturbative accelerations are caused by gravitational acceleration (up to J_2 contribution), atmospheric drag (Harris-Priester model) and solar radiation pressure acceleration. The sailcraft with a mass of 4 kg and sail area of 25 m^2, was assumed to be a rigid body without internal moving parts, in a sun synchronous orbit with the altitude of 620 km. As shown in Figure 2, the conclusion of the research presented that the nano-satellite sail system re-enters the atmosphere after 12 days.

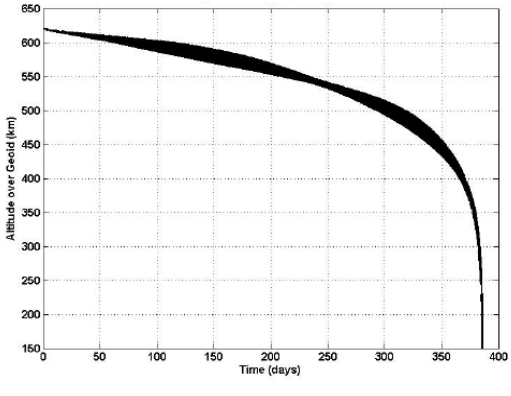

Figure 1. Spacecraft altitude over time for a 620 km SSO orbit

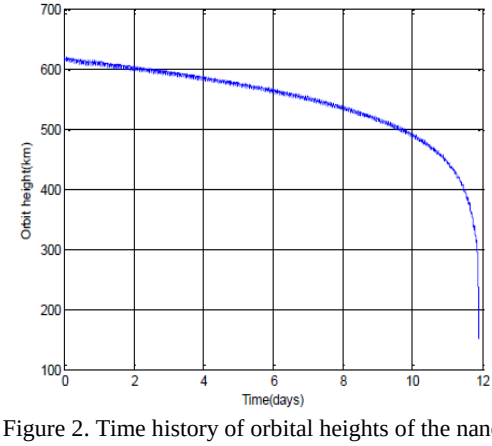

Figure 2. Time history of orbital heights of the nano-satellite with solar sail [3]

3. NUMERICAL INVESTIGATION DESCRIPTION

The current study focuses on assessing the feasibility of using a solar sail for deorbiting an upper stage at end-of-mission (EOM) in low Earth orbit (LEO). The numerical investigation is performed via a MATLAB simulation, projecting in time the orbital trajectory of the upper stage equipped with the solar sail. The orbital evolution is done using the *ode45* function in MATLAB, which integrates over time the accelerations acting upon the spacecraft, namely geopotential, atmospheric drag, solar radiation pressure (SRP) and indirect solar radiation pressure (iSRP). The shadow effect of the Earth and Moon are taken into account and two cases relating to solar sail efficiency are studied, namely *solar pressure* and *drag augmentation.*

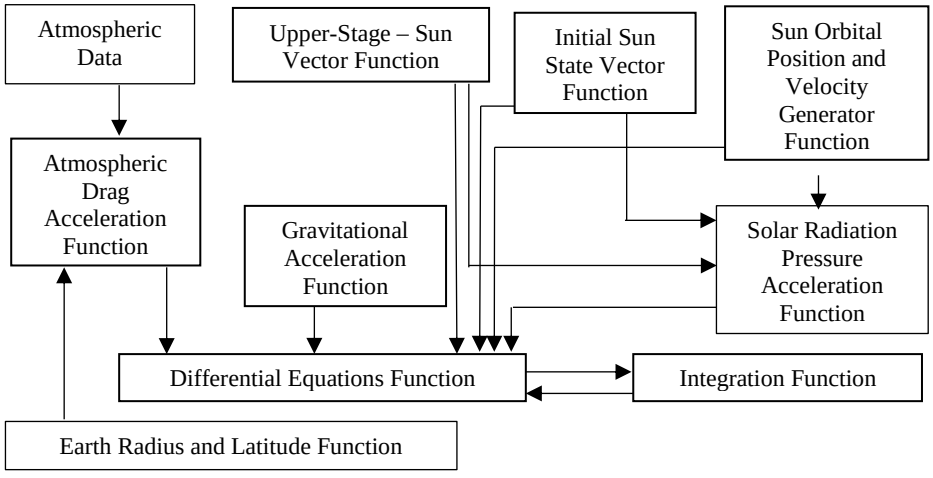

Figure 3. MATLAB Numerical Simulation Methodology Scheme

The MATLAB code, Figure 3, works by integrating with respect to time a second order differential equation (1) using the *ode45* solver. The equation uses as initial values the upper-stage state vector (2) and (3).

$$\dot{\boldsymbol{v}}_{us} = \boldsymbol{g}_{\boldsymbol{us}} - \frac{\boldsymbol{v}_{\boldsymbol{us}}}{\|\boldsymbol{v}_{\boldsymbol{us}}\|} a_{drag} + \frac{\boldsymbol{r}_{\boldsymbol{us-Sun}}}{\|\boldsymbol{r}_{\boldsymbol{us-Sun}}\|} a_{SRP} \tag{1}$$

$$\boldsymbol{X}_{us} = [\boldsymbol{r}_{us} \quad \boldsymbol{v}_{us}] = [\boldsymbol{x}_{us} \quad \boldsymbol{y}_{us} \quad \boldsymbol{z}_{us} \quad \boldsymbol{v}_{\boldsymbol{x}_{us}} \quad \boldsymbol{v}_{\boldsymbol{y}_{us}} \quad \boldsymbol{v}_{\boldsymbol{z}_{us}}] \tag{2}$$

$$\dot{\boldsymbol{X}}_{us} = [\dot{\boldsymbol{r}}_{us} \quad \dot{\boldsymbol{v}}_{us}] = [\dot{\boldsymbol{x}}_{us} \quad \dot{\boldsymbol{y}}_{us} \quad \dot{\boldsymbol{z}}_{us} \quad \dot{\boldsymbol{v}}_{\boldsymbol{x}_{us}} \quad \dot{\boldsymbol{v}}_{\boldsymbol{y}_{us}} \quad \dot{\boldsymbol{v}}_{\boldsymbol{z}_{us}}] \tag{3}$$

The constants shown in Table 1 have been used in the calculation of the gravitational acceleration.

Table 1. Constants used in the geopotential model

Mass of Earth	$M_E = 5.972 \cdot 10^{24}\ kg$
Earth Equatorial Radius	$R_E = 6372.137\ km$
Gravitational Constant	$G = 6.673 \cdot 10^{-20} km^3/kg \cdot s$
J2 Parameter	$J_2 = 1.08263 \cdot 10^{-3}$
J3 Parameter	$J_3 = -2.5321 \cdot 10^{-6}$
J4 Parameter	$J_4 = -1.610987 \cdot 10^{-6}$

Equations (4) – (15) are components of a function used to calculate the gravitational acceleration having the spacecraft position vector as input, [7]. The function outputs the gravitational acceleration in the x, y, z directions, for which (13), (14) and (15) are used. These outputs are used by the *ode45* solver and integrated with respect to time.

$$R_{mag} = \|\boldsymbol{r_{us}}\| \tag{4}$$

$$R_{R2} = \left(\frac{R_E}{R_{mag}}\right)^2 \tag{5}$$

$$R_{R3} = \left(\frac{R_E}{R_{mag}}\right)^3 \tag{6}$$

$$R_{R4} = \left(\frac{R_E}{R_{mag}}\right)^4 \tag{7}$$

$$z_R = \frac{\boldsymbol{z_{us}}}{R_{mag}} \tag{8}$$

$$z_{R2} = \left(\frac{\boldsymbol{z_{us}}}{R_{mag}}\right)^2 \tag{9}$$

$$z_{R4} = \left(\frac{\boldsymbol{z_{us}}}{R_{mag}}\right)^4 \tag{10}$$

$$q = 1 + 1.5 \cdot J_2 \cdot R_{R2}(1 - 5z_{R2}) + 2.5 \cdot J_3 \cdot R_{R3}(3 - 7z_{R2})z_R - 4.375 \cdot J_4 \cdot R_{R4}\left(9z_{R4} - 6z_{R2} + \frac{3}{7}\right) \tag{11}$$

$$\mu = G_E M_E \tag{12}$$

$$g_x = -\frac{\mu}{R_{mag}^3}\boldsymbol{x_{us}}q \tag{13}$$

$$g_y = -\frac{\mu}{R_{mag}^3}\boldsymbol{y_{us}}q \tag{14}$$

$$g_z = -\frac{\mu}{R_{mag}^2}\left\{\left[\left(1 + 1.5J_2R_{R2}(3 - 5z_{R2})\right)z_R + \left(2.5J_3R_{R3}(6z_{R2} - 7z_{R4} - 0.6)\right) + \left(-4.375J_4R_{R4}\left(\frac{15}{7} - 10z_{R2} + 9z_{R4}\right)z_R\right)\right]\right\} \tag{15}$$

(16) is used for the determination of the acceleration caused by the atmospheric drag force, in which CD is the drag coefficient and ρ is the atmospheric density taken from [9] and [10].

$$a_{Drag} = -\frac{1}{2m}CDA\rho {v_{us}}^2 \frac{\boldsymbol{v_{us}}}{v_{us}} \tag{16}$$

Equation (17), from [6], was used for the calculation of the magnitude of the solar radiation pressure. $\beta = 0.15$ is the coefficient of reflection of reflection of black Kapton, the solar sail material, S_F is the solar flux which was calculated using (18), $P_S = 3.805 \cdot 10^{20}\ W$ is the radiative power of the Sun, r_S is the upper-stage – Sun distance, $a_e = 149.6 \cdot 10^6\ km$ is Earth's semi-major axis in heliocentric orbit, $c = 299\,792.458\ km/s$, A is the surface area of the solar sail, m is the mass of the upper-stage, the solar sail and additional equipment, $a_S = 149\ \times\ 10^6\ km$ is the Sun-Earth semi-major axis.

$$R = (1+\beta)\frac{S_F}{c}\frac{A\cos\alpha}{m}\left(\frac{a_S}{r_S}\right)^2 \tag{17}$$

$$S_F = \frac{P_S}{4\pi a_e^2} \tag{18}$$

For the solar pressure (SP) and drag augmentation (DA) cases, the solar radiation pressure acceleration acting upon the solar sail was considered null when the angle between the Sun-Earth vector and the spacecraft-Earth vector was outside the (-90°, 90°) interval, because the spacecraft would be pushed outside the orbit, not towards Earth. The Sun's orbital position was calculated with the (19) – (28) algorithm. In the case of the solar pressure effect, the solar sail normal vector is always aligned with the Earth – upper-stage position vector. In this case, the total area of the solar sail which is lit by the Sun and will contribute to the actual SRP value is found out by multiplying the area of the sail with the cosines of the angle between the upper-stage orbital velocity and the upper-stage – Sun vector. It is considered that the solar sail is aligned with the upper-stage orbital velocity. The purpose of the SRP effect is to push the upper-stage towards Earth. In the case of drag augmentation effect, the solar sail normal vector is always aligned with the upper-stage orbital velocity. In this case, the total area of the solar sail which is lit by the Sun and will contribute to the actual SRP value is found by multiplying the area of the sail with the cosines of the angle between the upper-stage – Earth position vector and the upper-stage – Sun vector. The purpose of the drag augmentation effect is to decelerate the upper-stage by pushing it with the sun lit in the opposite way that it is heading. The Sun's state vector is calculated at each instant using (19) and (20) having supplied the initial values $\boldsymbol{r}_{M_0}$ and $\boldsymbol{v}_{M_0}$, [8]. f and g in (21) and (22) represent the Lagrange coefficient with $\dot{f}$ and $\dot{g}$ being their time derivatives. $C(z)$ and $S(z)$ are *Stumpff* functions, χ represents the universal anomaly, which at $t_0 = 0$ is $\chi_{t_0} = 0$. μ_M is the Sun's gravitational parameter and takes the value $\mu_M = G(M_E + M_M)$ with $M_M = 0.0732 \times 10^{24}\, kg$.

$$\boldsymbol{r}_M = f\boldsymbol{r}_{M_0} + g\boldsymbol{v}_{M_0} \tag{19}$$

$$\boldsymbol{v}_M = \dot{f}\boldsymbol{r}_{M_0} + \dot{g}\boldsymbol{v}_{M_0} \tag{20}$$

$$f = 1 - \frac{\chi^2}{r_{M_0}}C(z) \tag{21}$$

$$g = \Delta t - \frac{1}{\sqrt{\mu}}\chi^3 S(z) \tag{22}$$

$$\dot{f} = \frac{\sqrt{\mu}}{r_M r_{M_0}}[z\chi S(z) - \chi] \tag{23}$$

$$\dot{g} = 1 - \frac{\chi^2}{r}C(z) \tag{24}$$

$$z = \frac{1}{a_M}\chi^2 \tag{25}$$

$$S(z) = \begin{cases} \sqrt{z} - \operatorname{Sin}\sqrt{z}, z > 0 \\ \operatorname{Sin}\sqrt{-z} - \sqrt{-z}, z < 0 \\ \frac{1}{6}, z = 0 \end{cases} \tag{26}$$

$$C(z) = \begin{cases} \dfrac{1-\cos\sqrt{z}}{z}, z > 0 \\ \dfrac{\cosh\sqrt{-z}-1}{-z}, z < 0 \\ \dfrac{1}{2}, z = 0 \end{cases} \quad (27)$$

$$\chi_{i+1} = \chi_i - \frac{\frac{r_0 v_{r0}}{\sqrt{\mu}}\chi_i{}^2 C(z_i) + \left(1 - \frac{1}{a_M} r_0\right)\chi_i{}^3 S(z_i) + r_0\chi_i - \sqrt{\mu}\Delta t}{\frac{r_0 v_{r0}}{\sqrt{\mu}}\chi_i\left[1 - \frac{1}{a_M}S(z_i)\right] + \left(1 - \frac{1}{a_M} r_0\right)\chi_i{}^2 C(z_i) + r_0} \quad (28)$$

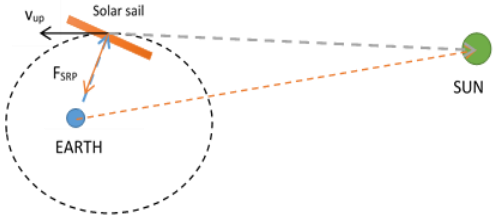

Figure 4. Solar Pressure (SP) effect case

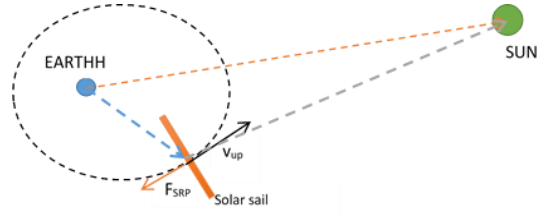

Figure 5. Drag augmentation (DA) effect case

For the determination of the Sun's initial state vector, a separate MATLAB function was created and the constants in Table 2 were used. For simplicity, it was considered that the Sun orbited the Earth and the Sun was considered to have initially the state vector with opposite sign of the Earth at perigee on the solar orbit.

Table 2. Constants used inside the MATLAB function for calculating the Sun orbital position around the Earth

Mass of Sun	$M_S = 1.989 \cdot 10^{30}\ kg$
Mass of Earth	$M_E = 5.9726 \cdot 10^{24}\ kg$
Global Gravitational Constant	$G = 6.673 \cdot 10^{-20}\ km^3/kg \cdot s$
Earth orbital semi-major axis	$a_S = 149.6 \cdot 10^6\ km$
Earth orbit periapsis	$p_E = 147.09 \cdot 10^6\ km$
Earth orbit apoapsis	$a_E = 152.1 \cdot 10^6\ km$
Earth orbit eccentricity	$e_S = 0.0167$
Earth axis tilt (Sun orbital inclination)	$i_S = 23.4°$
Argument of periapsis	$\omega_S = 102.947°$
Argument of ascending node	$\Omega_S = -11.26°$
Unit vector for non-rotated z axis	$k = [0 \quad 0 \quad 1]$

(29) – (38) present the formulation used for the gravitational parameter (29), the orbital angular momentum calculated at periapsis (30), the velocity of the Sun on orbit at periapsis (31), the initial non rotated position vector (32), the rotation matrix for the argument of periapsis rotation (33), the rotation matrix for the inclination rotation (34), the rotation matrix for the argument of ascending node rotation (35), the rotation equation (36), the equation for rotation around the Z axis (37), and the equation for determining the initial velocity (38).

$$\mu_S = G(M_S + M_E) \quad (29)$$

$$h = \sqrt{p_E \mu_S (1 + e_S \cos 0)} \quad (30)$$

$$v_{pE} = \frac{h}{p_E} \quad (31)$$

$$R_E = [-p_E \quad 0 \quad 0] \quad (32)$$

$$R_{\omega} = \begin{bmatrix} \cos\omega_S & \sin\omega_S & 0 \\ -\sin\omega_S & \cos\omega_S & 0 \\ 0 & 0 & 1 \end{bmatrix} \tag{33}$$

$$R_i = \begin{bmatrix} 1 & 0 & 0 \\ 0 & \cos i & \sin i \\ 0 & -\sin i & \cos i \end{bmatrix} \tag{34}$$

$$R_{\Omega} = \begin{bmatrix} \cos\Omega_S & \sin\Omega_S & 0 \\ -\sin\Omega_S & \cos\Omega_S & 0 \\ 0 & 0 & 1 \end{bmatrix} \tag{35}$$

$$R_{RE} = R_{\omega} R_i R_{\Omega} R_E \tag{36}$$

$$k_E = R_{\omega} R_i R_{\Omega} k \tag{37}$$

$$V_E = v_{pE}\left(\boldsymbol{k_E} \otimes \frac{\boldsymbol{R_E}}{\|\boldsymbol{R_E}\|}\right) \tag{38}$$

The orbital elements at each instant must be determined for a better understanding of the perturbing SRP and atmospheric drag. The following algorithm defines the orbital elements, where r is the Earth – upper-stage distance, v is the upper-stage's orbital speed, v_r is the upper-stage's radial speed, $\boldsymbol{h}$ is the upper-stage's orbital angular momentum, $\boldsymbol{N}$ is the vector node line of the upper-stage's orbit, Ω is the right ascension of the ascending node, $\boldsymbol{e}$ is the upper-stage's orbit eccentricity vector, ω is the upper-stage's orbit argument of periapsis, θ is the upper-stage's orbit true anomaly, a is the upper-stage's orbit semi-major axis, T is the upper-stage's orbital period and M is the upper-stage's orbit mean anomaly.

$$r = \sqrt{\boldsymbol{r} \cdot \boldsymbol{r}} \tag{39}$$

$$v = \sqrt{\boldsymbol{v} \cdot \boldsymbol{v}} \tag{40}$$

$$v_r = \frac{\boldsymbol{r} \cdot \boldsymbol{v}}{r} \tag{41}$$

$$\boldsymbol{h} = \boldsymbol{r} \times \boldsymbol{v} = \begin{vmatrix} \hat{\boldsymbol{\imath}} & \hat{\boldsymbol{\jmath}} & \hat{\boldsymbol{k}} \\ X & Y & Z \\ v_X & v_Y & v_Z \end{vmatrix} \tag{42}$$

$$h = \sqrt{\boldsymbol{h} \cdot \boldsymbol{h}} \tag{43}$$

$$i = \mathrm{Cos}^{-1}\left(\frac{h_Z}{h}\right) \tag{44}$$

$$\boldsymbol{N} = \hat{\boldsymbol{k}} \times \boldsymbol{h} = \begin{vmatrix} \hat{\boldsymbol{\imath}} & \hat{\boldsymbol{\jmath}} & \hat{\boldsymbol{k}} \\ 0 & 0 & 0 \\ h_X & h_Y & h_Z \end{vmatrix} \tag{45}$$

$$N = \sqrt{\boldsymbol{N} \cdot \boldsymbol{N}} \tag{46}$$

$$\Omega = \begin{cases} \mathrm{Cos}^{-1}\left(\frac{N_X}{N}\right), & N_Y \geq 0 \\ 360° - \mathrm{Cos}^{-1}\left(\frac{N_X}{N}\right), & N_Y < 0 \end{cases} \tag{47}$$

$$\boldsymbol{e} = \frac{1}{\mu}\left[\left(v^2 - \frac{\mu}{r}\right)\boldsymbol{r} - r v_r \boldsymbol{v}\right] \tag{48}$$

$$e = \sqrt{\boldsymbol{e}\cdot\boldsymbol{e}} \tag{49}$$

$$\omega = \begin{cases} \mathrm{Cos}^{-1}\left(\dfrac{\boldsymbol{N}\cdot\boldsymbol{e}}{Ne}\right), & e_Z \geq 0 \\ 360° - \mathrm{Cos}^{-1}\left(\dfrac{\boldsymbol{N}\cdot\boldsymbol{e}}{Ne}\right), & e_Z < 0 \end{cases} \tag{50}$$

$$\theta = \begin{cases} \mathrm{Cos}^{-1}\left(\dfrac{\boldsymbol{e}\cdot\boldsymbol{r}}{er}\right), & v_r \geq 0 \\ 360° - \mathrm{Cos}^{-1}\left(\dfrac{\boldsymbol{e}\cdot\boldsymbol{r}}{er}\right), & v_r < 0 \end{cases} \tag{51}$$

$$a = \frac{h^2}{\mu}\frac{1}{1-e^2} \tag{52}$$

$$T = \frac{2\pi}{\sqrt{\mu}} a^{\frac{3}{2}} \tag{53}$$

$$M = \frac{2\pi}{T} \tag{54}$$

4. MATLAB SIMULATION RESULTS

In Table 3 there are presented the main results of the numerical simulations in MATLAB. As for deorbiting time, it can be seen that for low LEO orbits, namely for the deorbiting starting altitude of 600 km, the best performance comes from the 150 radius solar sail, when used in the drag augmentation (DA) scenario. In this case, the deorbiting is done in 8 hours. Overall, for all altitudes and solar sail radii, the device is efficient, complying to the '25 years' mitigation rule even when deorbiting from higher LEO orbits, namely from 1400 km, with a 25 m radius solar sail, using the solar pressure (SP) effect, in 260 days.

The drag augmentation effect proves overall to be more efficient than the solar pressure effect, but an operational mission combining the two would be efficient, especially considering using the solar pressure effect for higher altitudes, and the drag augmentation effect for lower altitudes. Below there is presented a detailed analysis of the accelerations variations for each case, as well as an orbital elements variation for the 1400 km case, for the 25 m radius solar sale, for the solar pressure effect case and drag augmentation effect case.

Table 3. Numerical simulations results

Study case	Altitude [km]	Solar Sail radius [m]	Deorbiting time
Solar Pressure effect (SP)	600	25	31 days
	600	75	4 days
	600	150	28 hours
	1400	25	260 days
	1400	75	45 days
	1400	150	8 days
Drag Augmentation effect (DA)	600	25	16 days
	600	75	3 days
	600	150	8 hours
	1400	25	63 days
	1400	75	10 days
	1400	150	3 days

In Figure 6, there are presented the results for the altitude variation over the course of the deorbiting with solar sails with radii of 25m, 75m and 150m, from an initial altitude of 600 km, considering the solar pressure (SP) effect case.

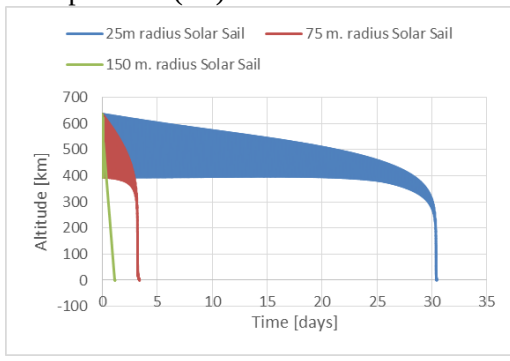

Figure 6. Deorbiting time when using solar sail of different sizes from an initial altitude of 600 km (SP effect)

In Figure 7 there are presented the results for the atmospheric drag acceleration variation over the course of the deorbiting with solar sails with radii of 25m, 75m and 150m, from an initial altitude of 600 km, considering the solar pressure (SP) effect case.

In Figure 8 there are presented the results for the solar radiation pressure variation over the course of the deorbiting with solar sails with radii of 25m, 75m and 150m, from an initial altitude of 600 km, considering the solar pressure (SP) effect case.

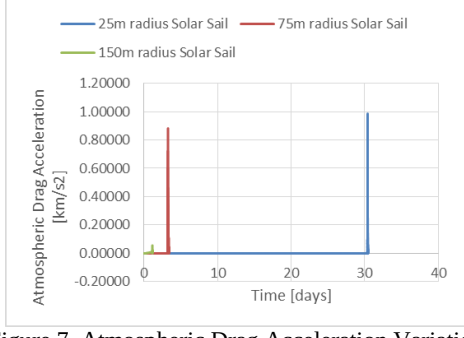

Figure 7. Atmospheric Drag Acceleration Variation when using solar sail of different sizes from an initial altitude of 600 km (SP effect)

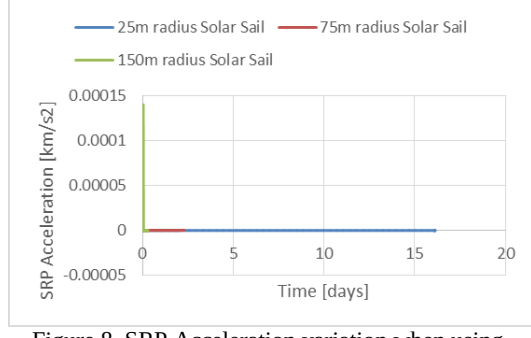

Figure 8. SRP Acceleration variation when using solar sails of different sizes from an initial altitude of 600 km (SP effect)

In Figure 9 there are presented the results for altitude variation over the course of the deorbiting with solar sails with radii of 25m, 75m and 150m, from an initial altitude of 600 km, considering the drag augmentation (DA) effect case.

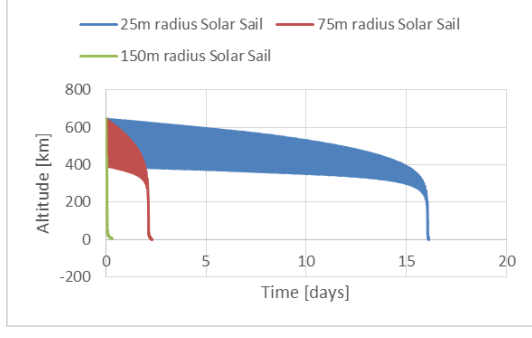

Figure 9. Altitude variation when using solar sails of different sizes from an initial altitude of 600 km (DA effect)

In Figure 10 there are presented the results for atmospheric drag acceleration variation over the course of the deorbiting with solar sails with radii of 25m, 75m and 150m, from an initial altitude of 600 km, considering the drag augmentation (DA) effect case. In Figure 11 there are presented the results for SRP acceleration variation over the course of the deorbiting with solar sails with radii of 25m, 75m and 150m, from an initial altitude of 600 km, considering the drag augmentation (DA) effect case.

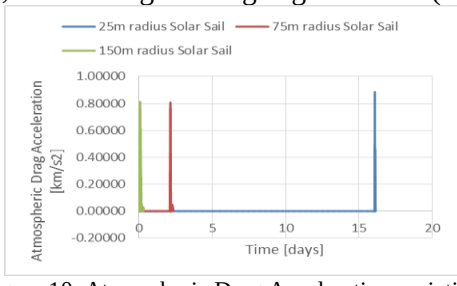

Figure 10. Atmospheric Drag Acceleration variation when using solar sails of different sizes from an initial altitude of 600 km (DA effect)

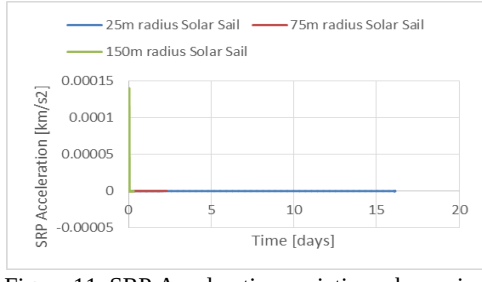

Figure 11. SRP Acceleration variation when using solar sails of different sizes from an initial altitude of 600 km (DA effect)

In Figure 12 there are presented the results for altitude variation over the course of the deorbiting with solar sails with radii of 25m, 75m and 150m, from an initial altitude of 1400 km, considering the solar pressure (SP) effect case.

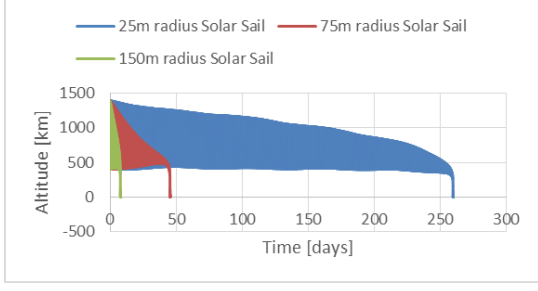

Figure 12. Altitude variation when using solar sails of different sizes from an initial altitude of 1400 km (SP effect)

In Figure 13 there are presented the results for atmospheric drag acceleration variation over the course of the deorbiting with solar sails with radii of 25m, 75m and 150m, from an initial altitude of 1400 km, considering the solar pressure (SP) effect case.

In Figure 14 there are presented the results for SRM acceleration variation over the course of the deorbiting with solar sails with radii of 25m, 75m and 150m, from an initial altitude of 1400 km, considering the solar pressure (SP) effect case.

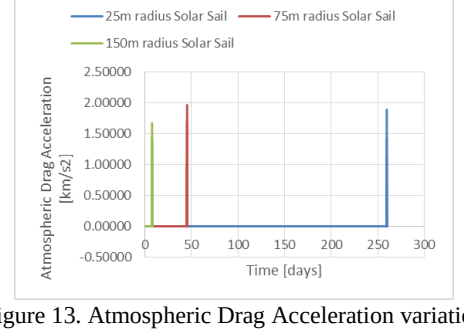

Figure 13. Atmospheric Drag Acceleration variation when using solar sails of different sizes from an initial altitude of 1400 km (SP effect)

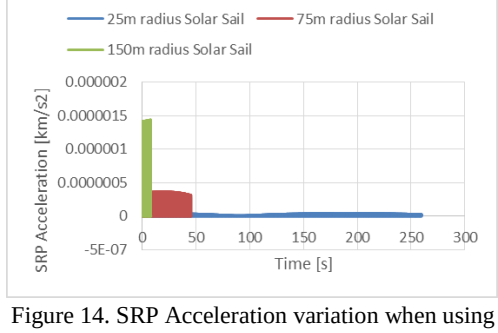

Figure 14. SRP Acceleration variation when using solar sails of different sizes from an initial altitude of 1400 km (SP effect)

In Figure 15 there are presented the results for inclination variation over the course of the deorbiting with solar sails with radius of 25m, from an initial altitude of 1400 km, considering the solar pressure (SP) effect case.

In Figure 16 there are presented the results for argument of periapsis variation over the course of the deorbiting with solar sails with radius of 25m, from an initial altitude of 1400 km, considering the solar pressure (SP) effect case.

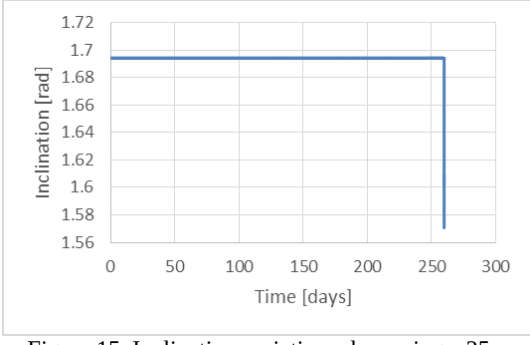

Figure 15. Inclination variation when using a 25m radius Solar Sail from an initial altitude of 1400 km (SP effect)

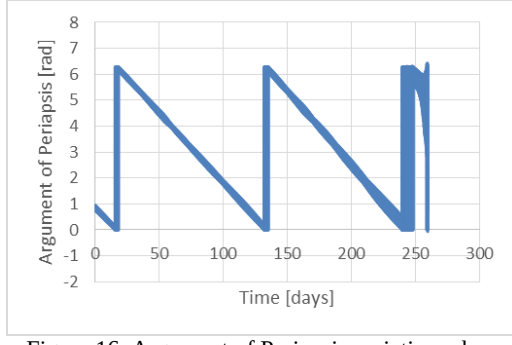

Figure 16. Argument of Periapsis variation when using a 25m radius Solar Sail from an initial altitude of 1400 km (SP effect)

In Figure 17 there are presented the results for true anomaly variation over the course of the deorbiting with solar sails with radius of 25m, from an initial altitude of 1400 km, considering the solar pressure (SP) effect case.

In Figure 18 there are presented the results for eccentricity variation over the course of the deorbiting with solar sails with radius of 25m, from an initial altitude of 1400 km, considering the solar pressure (SP) effect case.

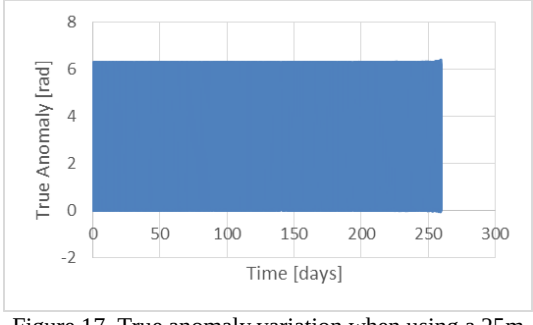

Figure 17. True anomaly variation when using a 25m radius Solar Sail from an initial altitude of 1400 km (SP effect)

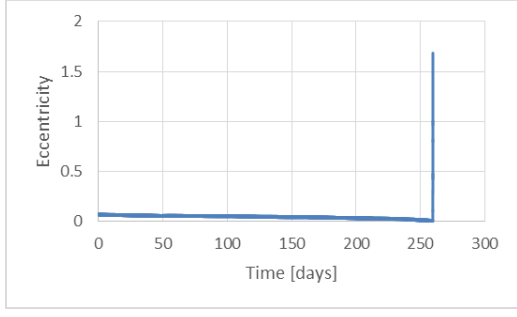

Figure 18. Eccentricity variation when using a 25m radius Solar Sail from an initial altitude of 1400 km (SP effect)

In Figure 19 there are presented the results for orbital angular momentum variation over the course of the deorbiting with solar sails with radius of 25m, from an initial altitude of 1400 km, considering the solar pressure (SP) effect case.

In Figure 20 there are presented the results for semi-major axis variation over the course of the deorbiting with solar sails with radius of 25m, from an initial altitude of 1400 km, considering the solar pressure (SP) effect case.

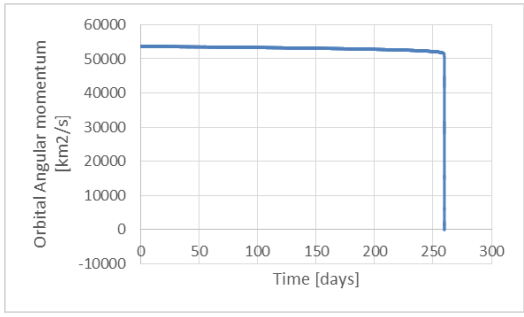

Figure 19. Orbital Angular Momentum variation when using a 25m radius Solar Sail from an initial altitude of 1400 km (SP effect)

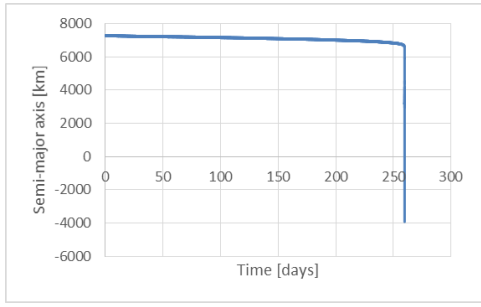

Figure 20. Semi-major Axis variation when using a 25m radius Solar Sail from an initial altitude of 1400 km (SP effect)

In Figure 21 there are presented the results for orbital period variation over the course of the deorbiting with solar sails with radius of 25m, from an initial altitude of 1400 km, considering the solar pressure (SP) effect case.

In Figure 22 there are presented the results for mean motion variation over the course of the deorbiting with solar sails with radius of 25m, from an initial altitude of 1400 km, considering the solar pressure (SP) effect case.

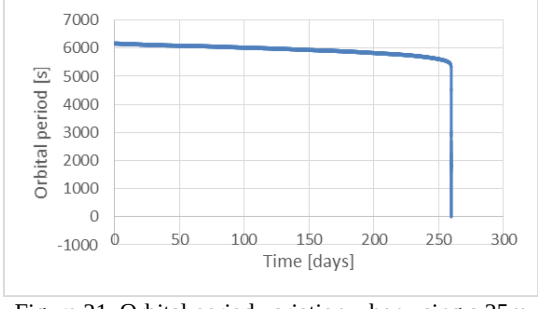

Figure 21. Orbital period variation when using a 25m radius Solar Sail from an initial altitude of 1400 km (SP effect)

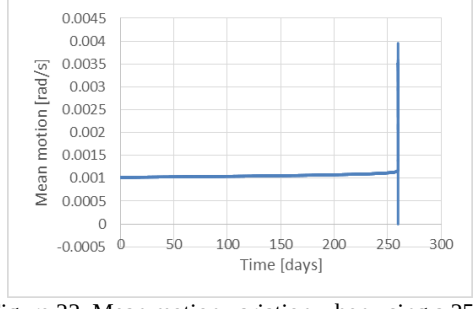

Figure 22. Mean motion variation when using a 25m radius Solar Sail from an initial altitude of 1400 km (SP effect)

In Figure 23 there are presented the results for altitude variation over the course of the deorbiting with solar sails with radii of 25m, 75m and 150m from an initial altitude of 1400 km, considering the drag augmentation (DA) effect case.

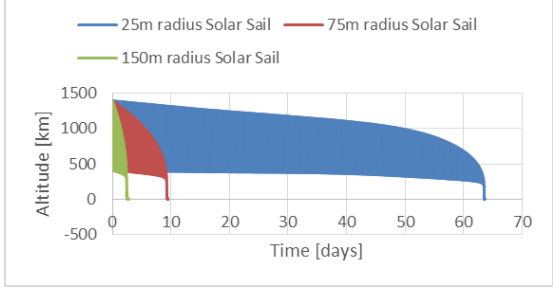

Figure 23. Altitude variation for solar sails of different sizes when deorbiting from an initial altitude of 1400 km (DA effect)

In Figure 24 there are presented the results for atmospheric drag acceleration variation over the course of the deorbiting with solar sails with radii of 25m, 75m and 150m from an initial altitude of 1400 km, considering the drag augmentation (DA) effect case. In Figure 25 there are presented the results for SRM acceleration variation over the course of the deorbiting

with solar sails with radii of 25m, 75m and 150m from an initial altitude of 1400 km, considering the drag augmentation (DA) effect case.

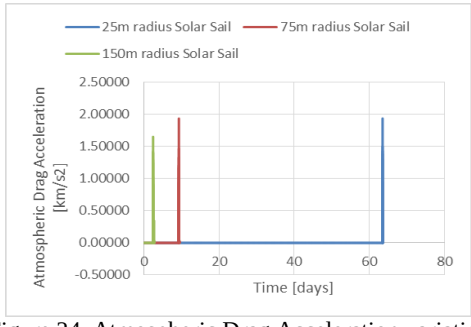

Figure 24. Atmospheric Drag Acceleration variation for solar sails of different sizes when deorbiting from an initial altitude of 1400 km (DA effect)

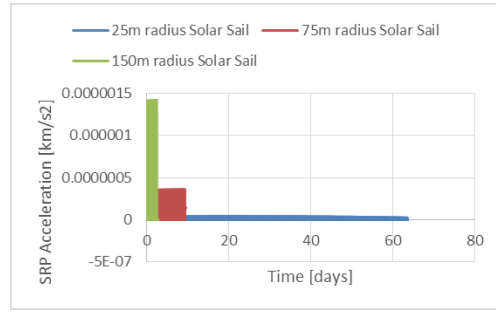

Figure 25. SRP Acceleration variation for solar sails of different sizes when deorbiting from an initial altitude of 1400 km (DA effect)

In Figure 26 there are presented the results for inclination variation over the course of the deorbiting with solar sails with radius of 25m, from an initial altitude of 1400 km, considering the drag augmentation (DA) effect case. In Figure 27 there are presented the results for argument of periapsis variation over the course of the deorbiting with solar sails with radius of 25m, from an initial altitude of 1400 km, considering the drag augmentation (DA) effect case.

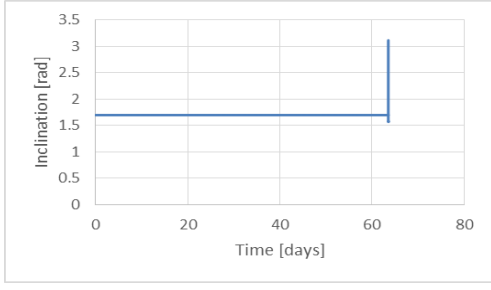

Figure 26. Inclination variation when using a 25m radius Solar Sail from an initial altitude of 1400 km (DA effect)

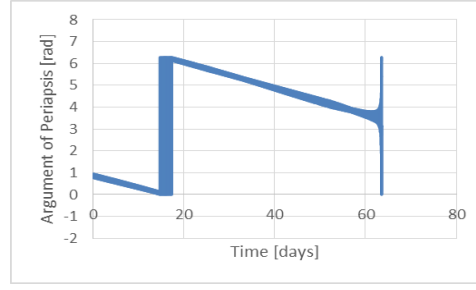

Figure 27. Argument of periapsis variation when using a 25m radius Solar Sail from an initial altitude of 1400 km (DA effect)

In Figure 28 there are presented the results for true anomaly variation over the course of the deorbiting with solar sails with radius of 25m, from an initial altitude of 1400 km, considering the drag augmentation (DA) effect case. In Figure 29 there are presented the results for eccentricity variation over the course of the deorbiting with solar sails with radius of 25m, from an initial altitude of 1400 km, considering the drag augmentation (DA) effect case.

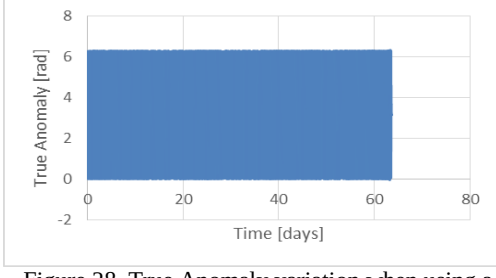

Figure 28. True Anomaly variation when using a 25m radius Solar Sail from an initial altitude of 1400 km (DA effect)

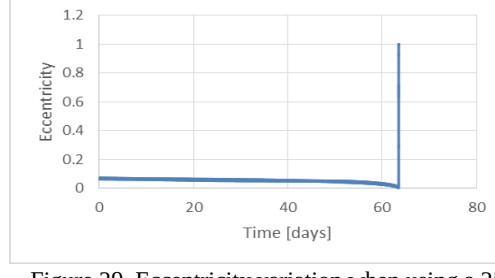

Figure 29. Eccentricity variation when using a 25m radius Solar Sail from an initial altitude of 1400 km (DA effect)

In Figure 30 there are presented the results for orbital angular momentum variation over the course of the deorbiting with solar sails with radius of 25m, from an initial altitude of 1400 km, considering the drag augmentation (DA) effect case.

In Figure 31 there are presented the results for semi-major axis variation over the course of the deorbiting with solar sails with radius of 25m, from an initial altitude of 1400 km, considering the drag augmentation (DA) effect case.

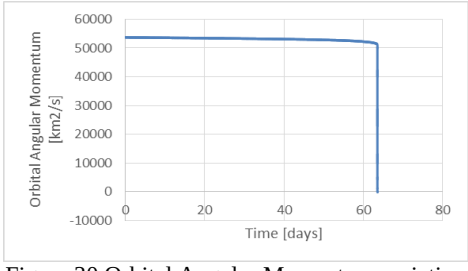

Figure 30 Orbital Angular Momentum variation when using a 25m radius Solar Sail from an initial altitude of 1400 km (DA effect)

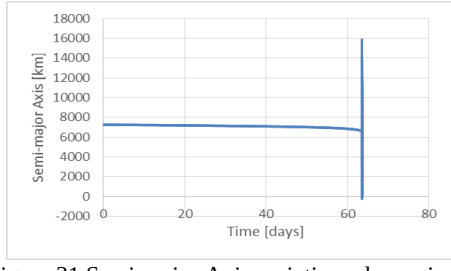

Figure 31 Semi-major Axis variation when using a 25m radius Solar Sail from an initial altitude of 1400 km (DA effect)

In Figure 32 there are presented the results for orbital period variation over the course of the deorbiting with solar sails with radius of 25m, from an initial altitude of 1400 km, considering the drag augmentation (DA) effect case.

In Figure 33 there are presented the results for mean motion variation over the course of the deorbiting with solar sails with radius of 25m, from an initial altitude of 1400 km, considering the drag augmentation (DA) effect case.

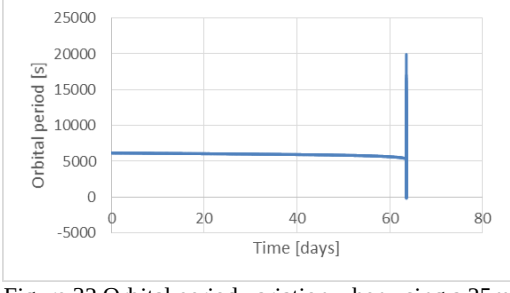

Figure 32 Orbital period variation when using a 25m radius Solar Sail from an initial altitude of 1400 km (DA effect)

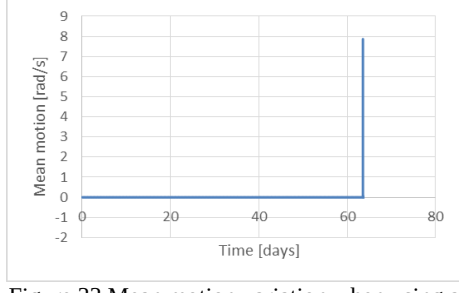

Figure 33 Mean motion variation when using a 25m radius Solar Sail from an initial altitude of 1400 km (DA effect)

5. CONCLUSIONS

The numerical simulations performed in this research paper have concluded the efficiency of a solar sail when used as a LEO deorbiting device. The study was concerned with the influence of solar radiation pressure and drag augmentation effects of the solar sail, for different sail dimensions and from the lower and upper LEO deorbiting altitudes. The results have shown that an upper-stage equipped with a solar deorbiting device deorbits from LEO within the ‘25 years’ mitigation rule.

The best results were obtained when using the solar sail with the drag augmentation effect, namely deorbiting being done in 8 hours with a 150m radius solar sail from 600 km altitude, and in 3 days with a 150m radius solar sail from 1400 km altitude. Future work will involve more complex deorbiting mission scenarios, solar sail attitude control studies, re-entry fragmentation studies and re-entry impact area calculations.

REFERENCES

[1] R. Thompson, A Space Debris Primer, *Crosslink*, Vol. **16**, No. 1, 2015.
[2] D. Romagnoli, S. Theil, De-orbiting Satellites in LEO using Solar Sails, *Journal of Aerospace Engineering, Sciences and Applications*, **IV** (2), pp. 49-59. ISSN 2236-577X, 2012.
[3] Y. Li, J. Zhang, Q. Hu, *Dynamics of Deorbiting of Low Earth Orbit Nano-Satellites by Solar Sail,* AAS 15-284.
[4] C. Lucking, C. Colombo, C. McInnes, *Solar Radiation Pressure Augmented Deorbiting from High Altitude Sun-Synchronous Orbits*, The 4S Symposium, 2012, Small Satellites Systems and Services - Portoroz, Slovenia.
[5] O. Tekinalp, O. Atas, *Attitude Control Mechanization to De-Orbit Satellites using Solar-Sails*, IAA-AAS-DyCoSS2-14-07-02.
[6] G. Bonin, J. Hiemstra, T. Sears, R. E. Zee, *The CanX-7 Drag Sail Demonstration Mission: Enabling Environmental Stewardship of Nano- and Microsatellites*, 27th Annual AIAA/USU Conference on Small Satellites SSC13-XI-9, 2013.
[7] A. Tewari, *Atmospheric and Space Flight Dynamics: Modeling and Simulation with MATLAB® and Simulink®*, Birkhäuser Basel ©2007, ISBN:0817643737 9780817643737.
[8] H. Curtis, *Orbital Mechanics for Engineering Students*, ISBN-13: 978-0080977478, ISBN-10: 0080977472, Elsevier, 2014.
[9] W. S. K. Champion, E. A. Cole and J. A. Kantor, *Standard and Reference Atmospheres*, Handbook of Geophysics and the Space Environment, Chapter 14, 2003.
[10] * * * *NASA, U.S. Standard Atmosphere*, 1976, N77-16482.